FEBS Letters 586 (2012) 557–567

journal homepage: www.FEBSLetters.org

Review

The catalytic domain of MMP-1 studied through tagged lanthanides

Ivano Bertini [a,b,*], Vito Calderone [a], Linda Cerofolini [a], Marco Fragai [a,b], Carlos F.G.C. Geraldes [c], Petr Hermann [d], Claudio Luchinat [a,b], Giacomo Parigi [a,b], João M.C. Teixeira [a,c]

[a] Magnetic Resonance Center (CERM), University of Florence, via Sacconi 6, 50019 Sesto Fiorentino, Italy
[b] Department of Chemistry, University of Florence, via Sacconi 6, 50019 Sesto Fiorentino, Italy
[c] Department of Life Sciences and Center of Neurosciences and Cell Biology, Faculty of Science and Technology, University of Coimbra, P.O. Box 3046, 3001-401 Coimbra, Portugal
[d] Department of Inorganic Chemistry, Faculty of Science, Univerzita Karlova (Charles University), Hlavova 2030, 12840 Prague 2, Czech Republic

ARTICLE INFO

Article history:
Received 30 June 2011
Revised 12 September 2011
Accepted 12 September 2011
Available online 19 September 2011

Edited by Miguel Teixeira and Ricardo O. Louro

Dedicated to António V. Xavier who pioneered the use of lanthanides in NMR in the early seventies. He exploited the potential of lanthanides as NMR probes for obtaining structural restraints for the conformational analysis of mononucleotides. His results are still inspiring nowadays researches, fulfilling the prediction that "this method will be capable of determining the structural properties in solution of a large number of biophysically interesting molecules" (Barry, C.D., North, A.C.T., Glasel, J.A., Williams, R.J.P. and Xavier, A.V. (1971) Quantitative determination of mononucleotide conformations in solution using lanthanide ion shift and broadening NMR probes. Nature 232, 236). Along these lines, the structural analysis of a biomolecule in solution is here performed through the use of the paramagnetic lanthanides.

Keywords:
Paramagnetic restraint
Paramagnetic tag
Lanthanide
Matrix metalloproteinase
Residual dipolar coupling

ABSTRACT

Pseudocontact shifts (pcs) and paramagnetic residual dipolar couplings (rdc) provide structural information that can be used to assess the adequacy of a crystallographic structure to represent the solution structure of a protein. This can be done by attaching a lanthanide binding tag to the protein. There are cases in which only local rearrangements are sufficient to match the NMR data and cases where significant secondary structure or domain rearrangements from the solid state to the solution state are needed. We show that the two cases are easily distinguishable. Whereas the use of solution restraints in the latter case is described in the literature, here we deal with how to obtain a better model of the solution structure in a case (the catalytic domain of the matrix metalloproteinase MMP-1) of the former class.

1. Introduction

A strategy proposed for monitoring and possibly improving the accuracy of a protein structure in solution is that of taking a crystal structure as a starting model and to validate or "correct" it by applying few, highly informative, long range NMR restraints [1–5]. Solution NMR data which are easily accessible are residual dipolar

* Corresponding author at: Magnetic Resonance Center (CERM), University of Florence, via Sacconi 6, 50019 Sesto Fiorentino, Italy.
E-mail address: ivanobertini@cerm.unifi.it (I. Bertini).

0014-5793/$36.00
doi:10.1016/j.febslet.2011.09.020

couplings, chemical shifts, and pseudocontact shifts in paramagnetic systems. By their own, these data are hardly able to determine the protein structure, and in any case the precision of the latter would not be comparable with that of the crystal structures. However, they can be used to monitor whether they are consistent within their experimental error with a crystal model: in positive cases, the crystal structure can be assumed to be accurate also in solution. Differently, these NMR data can be used as restraints to modify the model and obtain a more accurate structure in solution.

An early example of this strategy is provided by the use of pseudocontact shifts (pcs) from a paramagnetic ion in a metalloprotein [1]. Residual dipolar couplings (rdc) originating from external orienting media have also been proposed and highly successfully used [2,3]. More recently, a strategy based on the occurrence of a metal ion binding site – either natural or artificial – and the measurement of the paramagnetism-based pcs and rdc was proposed [5]. Protein structures were also calculated by modeling on other proteins with some homology in the primary sequence and refining the model through the paramagnetism-based restraints [6]. The paramagnetism-induced NMR restraints can actually provide valuable information for the structural and dynamic characterization of proteins [5,7–10] and, being long-range solution restraints, are particularly valuable for validating and refining a protein model.

The extent of the disagreement of the NMR restraints with the available model can be checked with a novel protocol that we have here implemented, based on anchoring the protein atoms to the coordinates of the model. In this way, the structural changes possibly needed to reproduce the experimental solution data are restricted to the minimum. Two cases can be encountered: (i) a good fit of the experimental data can be obtained with minor and uniformly distributed changes in the protein structure, or (ii) the experimental data remain in disagreement with the protein structure unless the latter is allowed to have sizable global conformational changes. In the first case, it is possible to conclude that the starting model is indeed close to the protein structure in solution. This information is highly relevant because even when the model is a crystal structure solved at high resolution, in many cases structural differences can arise in solution due to the absence of crystal packing forces and/or the possible presence of inhibitors bound to the protein. In the second case, i.e., when sizable global changes, like those involving secondary structural element rearrangements, are needed for obtaining a structure in agreement with the NMR data, different previously described approaches [2,4,5] should be applied. They are based on the use of force fields to keep the structure as close as possible to the original model, without restricting the possibility of sizable rearrangements under the driving force of the NMR restraints. Of course, the accuracy of the structure, as dictated by a few NMR restraints, is limited, but in any case better than that of the solid state model.

In this manuscript we show that the proposed protocol can discriminate between the two cases, by using the catalytic domain of the matrix metalloproteinase MMP-1 [11] and the protein calmodulin as representative examples. The structural analysis of the catalytic domain of MMP-1 was performed by solving the crystal structure of the protein, and by comparing the latter to the several structures deposited in the PDB with and without inhibitors. The paramagnetic NMR restraints (pcs and rdc) were acquired after the binding of a rigid lanthanide binding tag [12–21]. A number of paramagnetic lanthanide tags have been designed in the last years, to be rigidly attached to proteins, in order to take advantage of paramagnetism-assisted NMR for the structural and dynamic characterization of proteins and protein complexes. CLaNP-5 represents one of the last advances, showing no mobility nor multiple conformations [13,20,22]. This tag has been previously used for the study of the conformational heterogeneity of the complex formed by adrenodoxin reductase and its electron receiving partner adrenodoxin [23], and by cytochrome c and adrenodoxin [17]. Pcs and rdc resulted in agreement with the crystallographic model of the catalytic domain of MMP-1 after minor changes in the protein structure. On the opposite, in the case of calmodulin, we show that the same protocol can detect the presence of sizable structural changes occurring on passing from solid state to solution, when secondary structural elements assume different relative orientations [4,5].

2. Materials and methods

2.1. Sample preparation

2.1.1. CLaNP-5 (1,4,7,10-tetraazacyclododecane-1,7-[bis(N-oxido-pyridine-2-yl)methyl]-4,10-diyl-bis(2-(acetylamino)ethylmethane-sulfonothioate)) synthesis

The tag was synthesized as previously described [22,24], except that the last step consisted of functionalizing the compound precursor, 1,4,7,10-tetraazacyclododecane-1,7-[bis(N-oxido-pyridine-2-yl)methyl]-4,10-diacetic acid with (2-aminoethyl) methanethiosulfonate (MTS). The functionalization was achieved through reaction of the precursor with 2.3 equivalents MTS in the presence of 2 equivalents DMAP (4-dimethylaminopyridine), 1 equivalent HOBT (1-hydroxybenzotriazole), 4 equivalents TBTU O-(benzotriazol-1-yl)-*N,N,N′,N′*-tetramethyluronium tetrafluoroborate), and 5–6 equivalents DIPEA (*N*-ethyldiisopropylamin), and by stirring overnight at room temperature in dried acetonitrile. A HPLC purification step was then performed by using a Phenomenex C8 semi-preparative column (0.1% TFA, gradient 10–20% MeCN in H_2O). After lyophilisation of pure fraction (confirmed by analytical HPLC), a thick, slightly green colored solid was obtained, and the tag (CLaNP-5) stored at −20 °C.

2.1.2. Lanthanide binding to CLaNP-5

The tag was dissolved in DMF, incubated with an excess of a lanthanide(III) acetate salt (Ln^{3+} = Lu^{3+}, Yb^{3+}, Tm^{3+} or Tb^{3+}) at 32 °C, and shaken for 3 days. The unsoluble excess of lanthanide(III) salt was removed by centrifugation.

2.1.3. Protein expression and purification

The cDNA encoding sequence (Asn-106–Gly-261) of the catalytic domain of MMP-1 (CAT) was generated by the polymerase chain reaction (PCR), using the inactive full length MMP-1 gene (E219A) as template [11], and was cloned into pET21a by using NdeI and XhoI as restriction enzymes. The double mutation H132C/K136C, performed for the attachment of the CLaNP-5 tag, was engineered during a single PCR step using the QuickChange Site Directed Mutagenesis Kit (Stratagene): 5′-GCC AAG AGC AGA TGT GGA CTG TGC CAT TGA GTG TGC CTT CCA ACT CTG GAG-3′; 5′-CTC CAG AGT TGG AAG GCA CAC TCA ATG GCA CAG TCC ACA TCT GCT CTT GGC-3′. The mutations were confirmed by nucleotide sequencing. The expression vector was inserted into competent *Escherichia coli* BL21(DE3) CodonPlus RIPL strain cells, and the colonies were selected for ampicillin and chloramphenicol resistance. Single-labelled ^{15}N and doubly-labeled $^{13}C/^{15}N$ protein were expressed using minimal medium containing ^{15}N-enriched $(NH_4)_2SO_4$ and ^{13}C-enriched glucose (Cambridge Isotope Laboratories). Cell growth occurred at 37 °C, with induction at 0.6 O.D. with 500 μM of IPTG and harvested after 5 h expression. CAT MMP-1, precipitated as inclusion bodies, was solubilized, after lysis of the cells, in a solution of 8 M urea, 20 mM dithiothreitol, and 20 mM Sigma–Aldrich Trizma-base (pH 8), and stored at −20 °C. The refolding of CAT MMP-1 involved decreasing the urea gradient at 4 °C. The desired amount of protein was diluted into a 500 ml solution containing 6 M urea, 50 mM Trizma-base, 10 mM $CaCl_2$, 0.1 mM $ZnCl_2$, and 20 mM Cysteamine, at pH 8.0. The solution was then dialyzed against 1) 4 l of 4 M urea, 50 mM Trizma-base pH 8.0, 10 mM $CaCl_2$

and 0.1 mM $ZnCl_2$; 2) 4 l of 2 M urea, 50 mM Trizma-base pH 7.2, 10 mM $CaCl_2$, 0.1 mM $ZnCl_2$, and 0.3 M NaCl; 3) three steps of 20 mM Trizma-base pH 7.2, 10 mM $CaCl_2$, 0.1 mM $ZnCl_2$, and 0.3 M NaCl. The resulting 500 ml protein sample was concentrated down to 100 ml using MiniKros Modules (Spectrumlabs). CAT MMP-1 was purified by using HiLoad 26/60 Superdex 75 pg (Amersham Biosciences). Protein pure stocks were stored at 4 °C.

2.1.4. CLaNP-5 attachment

An aliquot of 5 ml of 10 μM protein was dialyzed against anaerobic buffer (20 mM Trizma-base pH 7.2, 10 mM $CaCl_2$ and 0.1 mM $ZnCl_2$, 0.3 M NaCl) under anaerobic conditions. The protein was then treated with 20 mM of Dithiothreitol (DTT) to reduce the engineered cysteines. Still in anaerobic conditions the DTT was removed by using PD10 desalting columns, and the protein was concentrated down to 1 ml. 10 equivalents of tag CLaNP-5 were added to the sample; reaction proceeded overnight at 4 °C (20 mM Trizma-base pH 7.2, 10 mM $CaCl_2$ and 0.1 mM $ZnCl_2$, 0.3 M NaCl). Precipitation was observed after overnight incubation. Final buffer conditions were obtained by washing the sample with PD10 desalting columns against 20 mM Trizma-base pH 7.2, 10 mM $CaCl_2$ and 0.1 mM $ZnCl_2$, 0.15 M NaCl. The final yield was around 60% due to protein precipitation. The NMR spectra showed that the protein is fully reacted with the metal complex.

2.1.5. Protein preparation for crystal structure determination

The wild type CAT MMP-1 was prepared as previously described [25].

2.2. Protein crystallization and structure determination

The protein samples were concentrated to 0.7 mM. Crystals of CAT MMP-1 were obtained under aerobic conditions by using the vapour diffusion technique at 289 K from solutions containing 0.1 M Tris–HCl pH 8.5 and 30% PEG 8000. The dataset was collected by using synchrotron radiation at DESY (EMBL, Hamburg) on beamline BW7A, at 100 K; the crystal used for data collection was cryo-cooled by using 20% ethylene glycol in the mother liquor.

The data were processed as monoclinic C2 by using the program MOSFLM [26] and scaled by using the program SCALA [27] with the TAILS and SECONDARY corrections on (the latter restrained with a TIE SURFACE command), to achieve an empirical absorption correction.

Table 1 shows the data collection and processing statistics for all datasets. The structure was solved by using the molecular replacement technique; the structure of collagenase-1 (PDB 966C) was used as a model, where water molecules and ions were omitted. The correct orientation and translation of the three molecules present in the asymmetric unit were determined with standard Patterson search techniques [28,29] as implemented in the program MOLREP [30,31]. The isotropic refinement was carried out by using REFMAC5 [32]. REFMAC5 default weights for the crystallographic and the geometrical term have been used in all cases.

In between the refinement cycles the models were subjected to manual rebuilding by using XtalView [33]. Water molecules were added by using the standard procedures within the ARP/WARP suite [34]. The stereochemical quality of the refined model was assessed by using the program Procheck [35].

2.3. NMR measurements

All experiments were performed on samples of a mutant (E219A, H132C, K136C) of CAT MMP-1 functionalized with the tag CLaNP-5 coordinated to a lanthanide ion (Lu^{3+}, Yb^{3+}, Tm^{3+} or Tb^{3+}), at concentrations ranging between 0.15 and 0.2 mM (20 mM Tris, pH = 7.2, 0.15 M NaCl, 0.1 mM $ZnCl_2$, 10 mM $CaCl_2$).

Table 1
Data collection and refinement statistics.

Space group	C2
Cell dimensions (Å, °)	a = 147.69, b = 54.53, c = 94.90, β = 120.69°
Resolution (Å)	51.4–2.2
Unique reflections	32 923 (4785)[a]
Overall completeness (%)	99.2 (99.2)
R_{sym} (%)	6.6 (49.1)
Multiplicity	3.0 (3.0)
$I/(\sigma I)$	9.1 (1.7)
Wilson plot B-factor (Å^2)	40.10
R_{cryst}/R_{free} (%)	22.4/28.8
Protein atoms	3730
Water molecules	196
Ions	15
RMSD bond lengths (Å)	0.020
RMSD bond angles (°)	2.40
Mean B-factor (Å^2)	36.34

[a] Numbers in parenthesis refer to high resolution shells.

All NMR experiments were performed at 310 K and acquired on Bruker AVANCE 700 and DRX 500 spectrometers, equipped with triple resonance cryo-probes. All spectra were processed with the Bruker TOPSPIN software packages and analyzed by the program CARA (Computer Aided Resonance Assignment, ETH Zurich) [36]. ^{1}H-^{15}N HSQC spectra were recorded at 500 MHz. The assignment of the protein functionalized with Lu-CLaNP-5 was obtained by the comparison of the ^{1}H-^{15}N HSQC spectrum with the assignment reported on BMRB [37] and the analysis of the 3D HNCA experiment performed at 700 MHz. The ^{1}H-^{15}N HSQC spectrum of Yb-CLaNP-5-CAT MMP-1 was assigned with the help of the 3D HNCA and CBCA(CO)NH experiments performed at 500 MHz. The ^{1}H-^{15}N HSQC of Tm-CLaNP-5- and Tb-CLaNP-5-CAT MMP-1 were assigned by using the other assigned spectra and pseudocontact shift predictions.

^{1}H-^{15}N residual dipolar couplings were measured at 310 K and 700 MHz for the CAT MMP-1 functionalized with the Tm-CLaNP-5 and Tb-CLaNP-5 tags by using the IPAP method [38]. In the case of the Yb-CLaNP-5 tag, due to the smaller magnetic susceptibility anisotropy of the metal, the measurements were performed on an Avance 900 MHz Bruker spectrometer to achieve a higher alignment of the protein, and thus larger rdc values.

2.4. Paramagnetism-based restraints

The electron-nucleus dipolar coupling does not average to zero upon rotation in the presence of anisotropy in the paramagnetic susceptibility tensor. A contribution to the hyperfine shift, which is called *pseudocontact shift* (pcs) thus arises, which is described by Eq. (1) [39]

$$pcs = \frac{1}{12\pi r^3}\left[\Delta\chi_{ax}(3\cos^2\theta - 1) + \frac{3}{2}\Delta\chi_{rh}\sin^2\theta\cos 2\varphi\right] \quad (1)$$

where r is the distance between observed nuclei and metal ion, $\Delta\chi_{ax}$ and $\Delta\chi_{rh}$ are the axial and rhombic anisotropy parameters of the magnetic susceptibility tensor of the metal, and θ and φ are the spherical angles defining the position of the nucleus in the frame of the paramagnetic susceptibility tensor. Therefore, pcs values depend only on the position of the nuclei with respect to the frame defined by the magnetic susceptibility tensor, with origin on the metal ion, and on the anisotropy values.

Rdc due to partial self-orientation of the paramagnetic protein in the magnetic field is described by Eq. (2) [39,40]

$$rdc\ (Hz) = -\frac{S_{LS}}{4\pi}\frac{B_0^2}{15kT} \times \frac{\gamma_N\gamma_H\hbar}{2\pi r_{HN}^3}\left[\Delta\chi_{ax}(3\cos^2\alpha - 1) + \frac{3}{2}\Delta\chi_{rh}\sin^2\alpha\cos 2\beta\right] \quad (2)$$

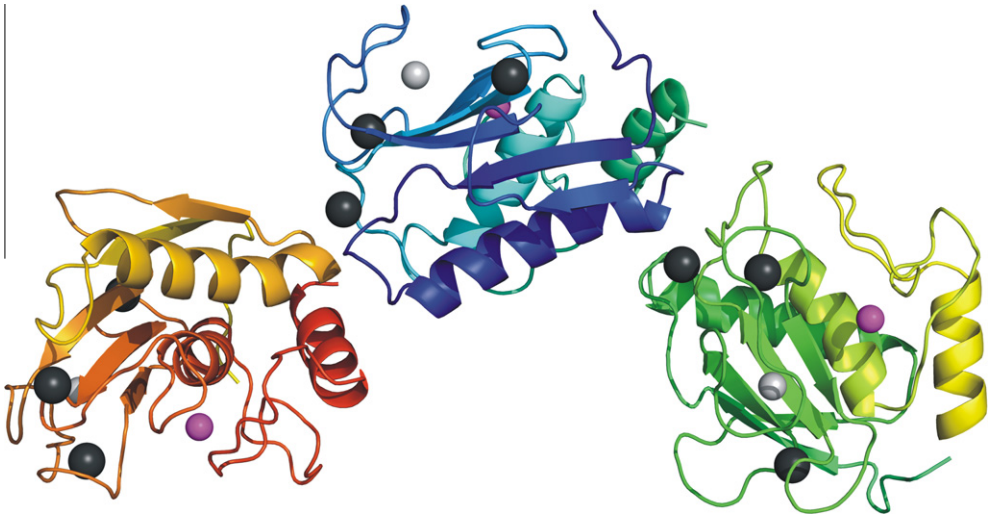

Fig. 1. Crystal structure of the catalytic domain of MMP-1. Structural zinc ions are in light grey, catalytic zinc ions are in magenta and calcium ions are in dark grey.

where r_{HN} is the distance between the two coupled nuclei N and ^{N}H (set equal to 1.02 Å) and the spherical angles α and β define the orientation of the vector connecting the coupled nuclei in the frame of the magnetic susceptibility tensor. S_{LS} is the model-free order parameter, introduced to take into account some local mobility of the nitrogen-amide proton vector. Other symbols have the usual meaning. Therefore, rdc values depend on the orientation of the vector connecting the coupled nuclei in the reference frame of the magnetic susceptibility tensor axes, on the values of the anisotropies of the latter, on the applied magnetic field and on the gyromagnetic ratio of the coupled nuclei [41–44]. They are not related at all to the position of the coupled nuclei with respect to both the metal ion and the magnetic susceptibility tensor.

3. Results and discussion

3.1. Crystallographic structure

The structure of the catalytic domain of wild type MMP-1 was solved at 2.2 Å resolution, and deposited in the PDB with code 3SHI. The space group is C2 and three molecules are present in the asymmetric unit (Fig. 1). The backbone RMSD between the different protein molecules in the unit cell is 0.25 Å. There are no regions showing significant lack of density involving the main chain of the three molecules in the asymmetric unit. The Ramachandran plot is of good quality (90.8% core, 8.4% allowed, 0.8% generously allowed and 0.0% disallowed residues). CAT MMP-1 is a "spherical" molecule that contains a twisted five-stranded β-sheet (I, II, III, IV and V) and three α-helices (A, B and C). The β-sheet contains four parallel strands and one antiparallel strand. The active site cleft is bordered by β-strand IV, helix B, and a stretch of random coil adjacent to the COOH terminus of helix B. The catalytic zinc is at the bottom of the cleft and is ligated by His 218, His 222, and His 228. In addition to the catalytic zinc, there is a second zinc ion that interacts with an extended loop between β-strand III and IV, and also three calcium atoms. Although the model used for molecular replacement contained all residues in trans conformation, the refinement provided two residues (Tyr A210 and Arg G108) in cis conformation.

The calculated structure 3SHI resulted similar to both the 1CGE crystal structure of the same protein without inhibitor already deposited in the PDB (the BB RMSD between the two structures is 0.44 Å in the residue range 108-261) and to the crystal structure at highest resolution (1HFC, resolution 1.56 Å), crystallized with a bulk hydroxamate inhibitor (with BB RMSD with 3SHI of 0.38 Å). The space group of these two structures is different from the C2 space group of 3SHI, as a result of different conditions of crystallization. The BB RMSD of 3SHI with the available solution structure (2AYK) is 1.34 Å. Also in 1HFC the residue Tyr A210 is in cis conformation, whereas in the other two structures all residues are in trans conformation.

In 1HFC, the space group is $P2_12_12_1$, with cell parameters different from those obtained in 3SHI. There are two small regions with significantly high RMSD between the 3SHI and the 1HFC structures (Fig. 2): the first one involves residues 188–190 and shows an RMSD of about 1 Å and the second one involves residues 242–245 with an RMSD which reaches 2.3 Å for residue 243 only. Both regions belong to protein loops; the second region belongs to the long loop forming the S_1' cavity. The regions which might be affected by the binding of the inhibitor in 1HFC are 178–182 and 238–240. These residues are not those with high RMSD, although they are adjacent. The high RMSD values can be determined by the presence of the inhibitor in 1HFC and by the different crystal contacts with symmetry related molecules present in the two space groups.

In the ligand-free 1CGE structure, the space group is $P4_12_12$, with one molecule in the asymmetric unit and different cell parameters with respect to the other mentioned structures. The superposition between the 3SHI and the 1CGE structures shows that residues 155–156 deviate by 1–2 Å, residues 243–244 deviate by 1–1.5 Å and residues 208 and 238 by slightly more than 1 Å. All other deviations are well below 1 Å. It is worth noticing that the region involving residues 178–182 does not show significant deviations (BB RMSD 0.3–0.4 Å), and that the deviations in the region 242–245 are much smaller than for the ligand-bound 1HFC structure.

3.2. Translating the protein model into a CYANA structure

Pcs and rdc provide structural information because they depend on the position of the observed nuclei and on the orientation of the vectors connecting coupled nuclei, respectively, in the frame defined by the paramagnetic susceptibility anisotropy tensor (see Eqs. (1) and (2)) [45]. They can thus be used for assessing whether an available structure is in agreement with these data, and possibly for calculating a solution structure in better agreement.

In order to estimate the extent of the structural changes needed to reproduce the paramagnetism-based restraints, the initial model was first adapted to fulfill all chemical bond constraints (in

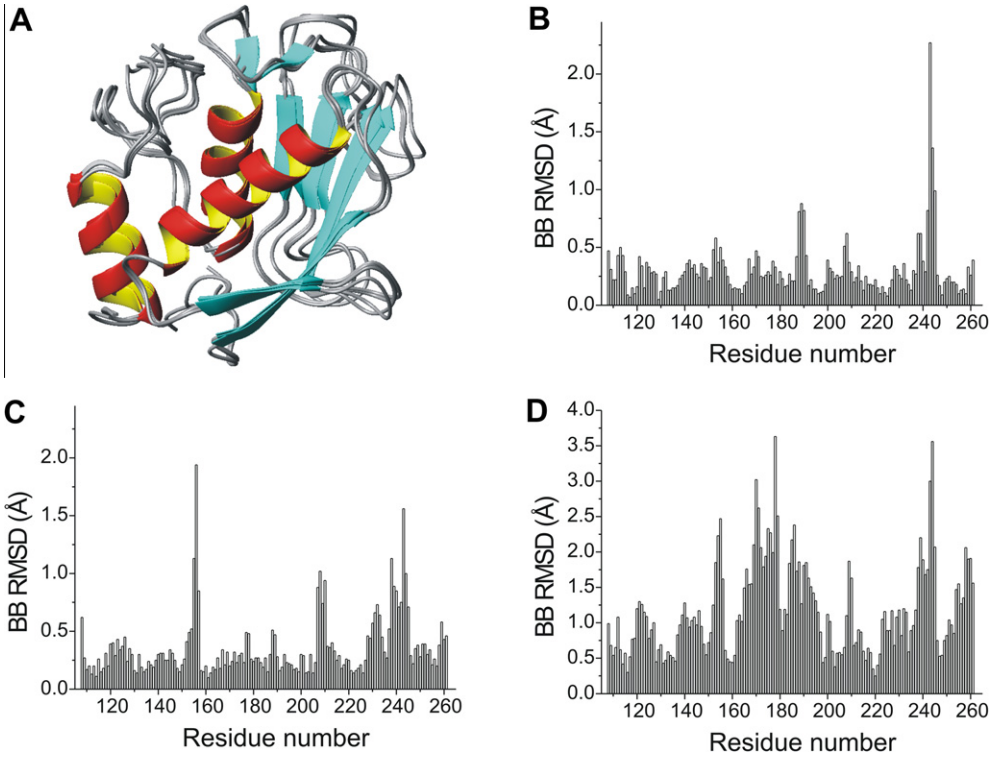

Fig. 2. (A) Superimposition of the four analyzed structures (the crystal structure 3SHI, here calculated, and the 1HFC, 1CGE and 2AYK structures). The bar plots represent the RMSD between the 3SHI and the (B) 1HFC, (C) 1CGE and (D) 2AYK structures.

terms of bond angles and lengths) of the library of the program CYANA [46]. This was done by including in the protein sequence a "pseudoprotein residue", composed by as many pseudoatoms as the number of atoms of the protein, each of them labeled according to its residue number and atom name. These pseudoatoms have coordinates equal to the coordinates of the corresponding atoms in the model structure and no van der Waals radius. The pseudoprotein residue was linked to the protein sequence through dummy residues, which have the function of allowing the pseudoprotein residue to freely move with respect to the protein residues. A simulated annealing calculation was performed with CYANA with upper distance limits of 0.1 Å (with weight 0.1) between all the heteroatoms of the protein and the corresponding atoms of the pseudoprotein residue. The dihedral ϕ and ψ angles were also restrained to vary within ±90° around the value in the model structure. A further conjugate gradient minimization was then performed with the same restraints and with the weight of the upper distance limits reduced to 0.01. In this way, the protein atoms are positioned as close as possible to the starting structure, being at the same time constrained to the bond lengths and angles defined in the internal library. This determined a slight rearrangement with respect to the four protein structures of CAT MMP-1 (3SHI, 1HFC, 2AYK, 1CGE), with backbone RMSD values to the starting structures of 0.25–0.30 Å.

3.3. Experimental NMR restraints

Pcs of ^{N}H nuclei and rdc of the ^{N}H–N pairs for the three paramagnetic Ln-CLaNP-5-CAT MMP-1 (Ln = Yb, Tm, Tb) forms were measured. Pcs restraints were first introduced into the CYANA calculation by using the routines dealing with the paramagnetic restraints available in PARAMAGNETIC CYANA [47]. They provided the metal position and the orientations of the magnetic anisotropy susceptibility tensors of the three metals. The metal ions were found at distances of 7.5 and 8 Å from the C^{α} nuclei of the tag-binding residues 132 and 136, respectively, in agreement with expectations based on previous results obtained with the same tag [22]. The magnitude of the anisotropy tensors (i.e., the $\Delta\chi ax$ and $\Delta\chi rh$ parameters) were obtained by cycling between PARAMAGNETIC CYANA and a minimization program performing a fit of the pcs data to the metal-containing protein structure. Pcs are indeed quite robust for providing the magnetic susceptibility anisotropy tensors (reported in Table 2), because they are not very sensitive to small local protein conformational changes, when the tag is rigidly bound to the protein (see later). The agreement between experimental and back-calculated pcs values is quite satisfactory for all four considered structures (see Fig. 3) with Q factors of 0.07–0.09. The fact that all pcs of the three metals agree simultaneously with a single protein structure, and that the anisotropy values are as high as expected for these metals, is an indication of both small internal mobility and rigidity of the attached tag. In fact, if the tag were largely mobile with respect to the protein, the metal-nucleus distances would average differently for the different nuclei, depending on their motion with respect to the magnetic susceptibility anisotropy tensors, and no average tensors could in principle be defined from the pcs values [5,48].

The agreement between experimental rdc values and rdc calculated with the pcs-derived tensors and either the initial structures or the structure calculated with CYANA was however unsatisfactory (Q factor = 0.72 for 3SHI). This may be due to the local mobility of each residue, to extensive mobility of the tag (which seems however excluded by the pcs, as discussed above), or to inaccuracies of the bond vector orientations in the available structure. A good estimation of the amide proton mobility can be obtained from ^{15}N relaxation rate measurements. R_1, R_2 and NOE measurements for the catalytic domain of MMP-1 are available [11] and actually indicate a sizable mobility for residues 108, 111, 116, 134, 135, 137, 145, 154, 157, 184, 191, 217, 227, 244, 245, 246, 249, 250, 260,

Table 2
Pcs-derived magnetic susceptibility anisotropy values for the three lanthanides and for the 3SHI, 1HFC, 1CGE and 2AYK structures, respectively.

	Yb^{3+}	Tm^{3+}	Tb^{3+}
$\Delta\chi ax$ (10^{32} m^3)	8.6, 8.0, 8.2 and 9.0	49.3, 47.4, 45.9 and 50.1	−44.9, −45.3, 43.4 and −44.6
$\Delta\chi rh$ (10^{32} m^3)	−2.1, −2.2, −2.8 and −3.0	−8.7, −8.6, −8.0 and −8.7	−20.1, −14.8, −14.5 and −11.5

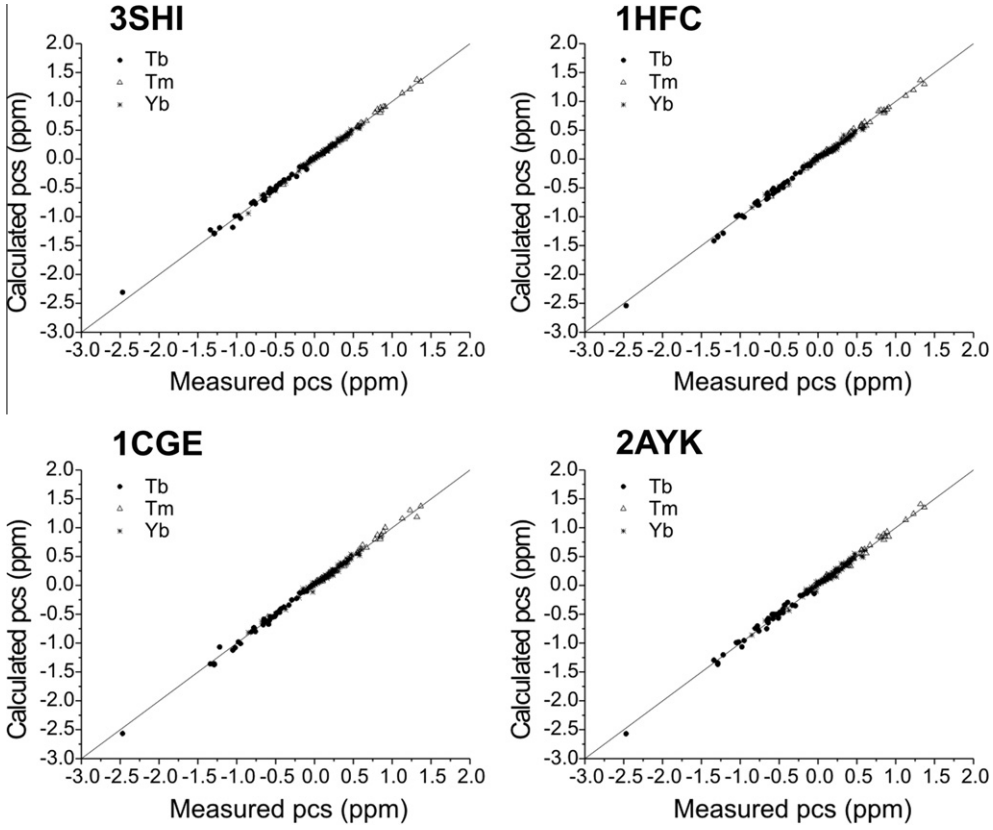

Fig. 3. Agreement between measured and calculated pcs obtained by using the magnetic susceptibility anisotropy parameters reported in Table 2 and the structures determined with PARAMAGNETIC CYANA, after the introduction of pcs and the upper distance limits for anchoring the protein nuclei to the nuclear coordinates of the 3SHI, 1HFC, 1CGE and 2AYK structures.

261. The rdc of these residues were thus excluded from all subsequent calculations. The Q factor of the remaining rdc is 0.67, 0.52, 0.69 and 0.83 for the 3SHI, 1HFC, 1CGE and 2AYK structures, respectively (Fig. 4A). The presence of a small mobility for the other residues can then be taken into account by including an order parameter S_{LS} (see Eq. (2)). The lowest Q factor was obtained for the rdc of the 1HFC structure, suggesting that this structure represents the best model in solution.

The rdc of non-mobile residues were fit to the 1HFC and 3SHI structures (see Fig. 4B) according to Eq. (2), with an order parameter S_{LS} fixed to 0.9 (fits of similar quality are obtained also with $S_{LS} = 1$) for all the values. The $\Delta\chi ax/\Delta\chi rh$ values were 7.1/−0.8, 39.7/−1.5, and −39.4/−16.7 × 10^{-32} m^3 for Yb^{3+}, Tm^{3+} and Tb^{3+}, respectively, for the 1HFC structure, and 7.0/−1.2, 36.6/−10.2, and −38.7/−10.4 × 10^{-32} m^3 for the 3SHI structure. The similar size of pcs- and rdc-derived tensors indicates that there is not a sizable global motion of the metal-bearing tag with respect to the protein, pointing out to its rigidity. The disagreement between calculated and experimental rdc is however outside the error (2 Hz) for many residues. This suggests that the H-^{H}N vectors of these residues experience a somewhat different conformation in solution with respect to these solid state structural models, which needs to be quantified. The rdc-derived tensors are actually expected to be somewhat reduced with respect to the pcs-derived tensors in the presence of inaccuracies in the relative orientation of the individual H–^{H}N vectors.

Therefore, rdc can be used for checking the consistency of the crystal model in solution by using the $\Delta\chi ax/\Delta\chi rh$ values determined from the pcs data. Remarkably, much worse fits of the rdc data were calculated for the crystal 1CGE structure as well as for the solution 2AYK structure (see Fig. 4B), although these two structures were obtained in the absence of inhibitors, again pointing out that they are less accurate models for the protein.

3.4. The protein solution structure

All pcs and rdc data (except the rdc of residues affected by large mobility, as shown by relaxation measurements) were introduced as restraints in the assumption that a unique tensor for any metal, and precisely that calculated from the pcs [5,8,39,49,50], is responsible for all the observed pcs and rdc values, as occurring in the absence of motion. The usual local mobility of H–^{H}N vectors was considered by using an order parameter S_{LS} of 0.9 for rdc. The weights of the restraints were 0.20 for Yb-rdc, 0.04 for the larger Tm- and Tb-rdc and 100 for pcs, which are much smaller in absolute value. Upper distance limits between the protein heteronuclei

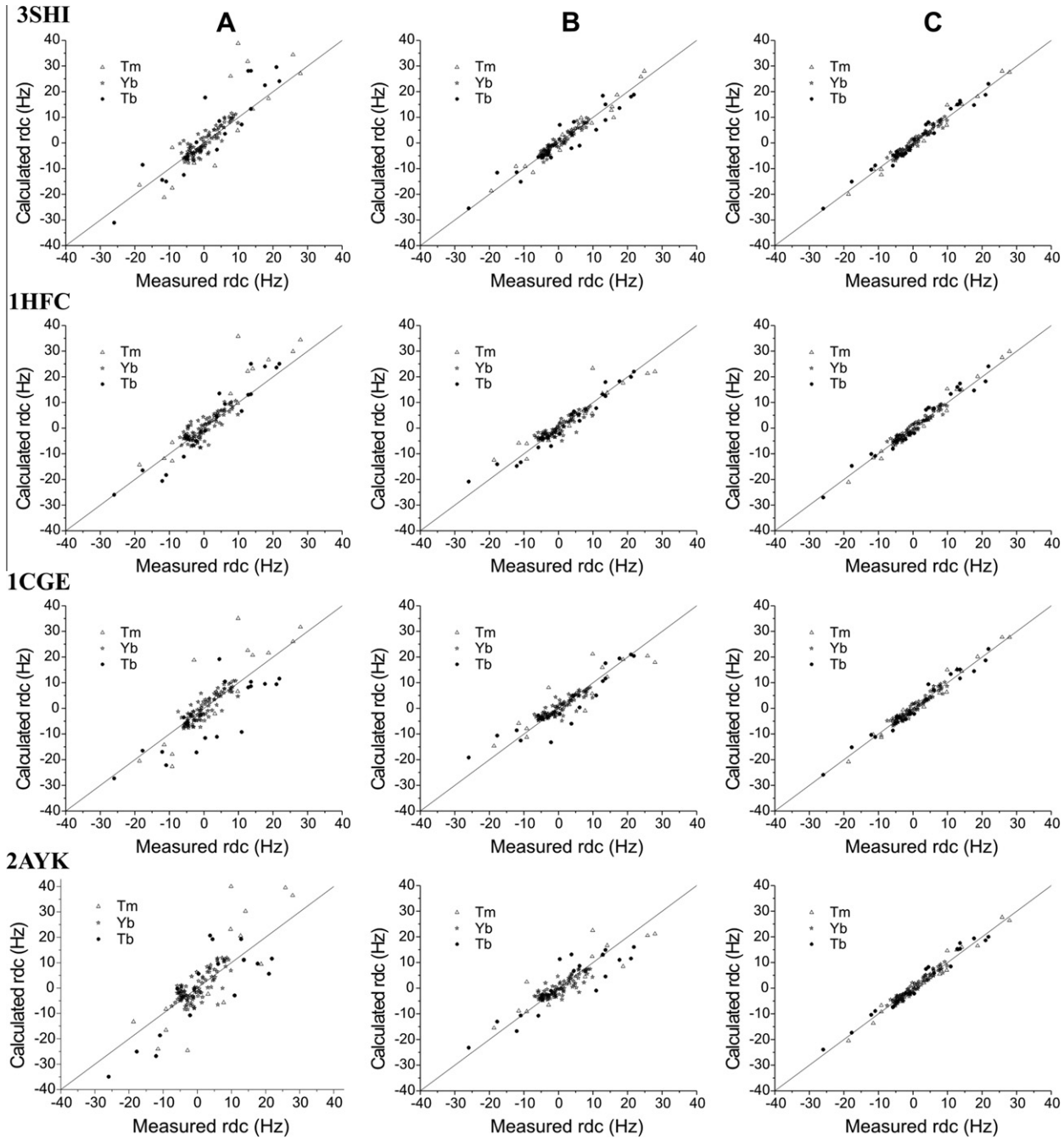

Fig. 4. (A) Agreement between experimental rdc and rdc calculated from the pcs-derived tensors and the 3SHI, 1HFC, 1CGE and 2AYK structures. (B) Best fit of the experimental rdc values to the 3SHI, 1HFC, 1CGE and 2AYK structures. (C) Agreement between experimental rdc and rdc calculated from the pcs-derived tensors and the solution structures.

and the pseudoatoms of the pseudoprotein residue were also included in the same way as described for the calculations in the absence of the paramagnetic restraints, for anchoring the position of the protein atoms to the coordinates of the selected model. A simulated annealing followed by a conjugated gradient minimization were performed with PARAMAGNETIC CYANA.

Because the 1HFC structure provides the best agreement with the paramagnetic data, as seen before, the calculation was first performed using this model. The resulting structure is shown in Fig. 5 together with the initial 1HFC crystal structure; the backbone RMSD between the two is 0.29 Å. The Ramachandran plot of the solution structure is still of very good quality (90.1% core, 9.9% allowed, 0.0% generously allowed and disallowed residues), without van der Waals contact violations, and with the bond length and angle parameters fixed to the library values of CYANA. Fig. 4C shows the good agreement between calculated and observed rdc values. The rdc Q factor decreases to 0.19 from 0.52.

Calculations were also performed using the 1CGE and 3SHI structures as models. For the structures so obtained, the agreement of the data is as good as that obtained for the 1HFC structure ($Q = 0.20$, versus 0.67 and 0.69), and the RMSD between the crystal and the corresponding solution structures is again lower than 0.4 Å.

The fact that single structures so similar to the crystal models are in very good agreement with the experimental data indicates that there is no need to invoke ensemble averaging approaches

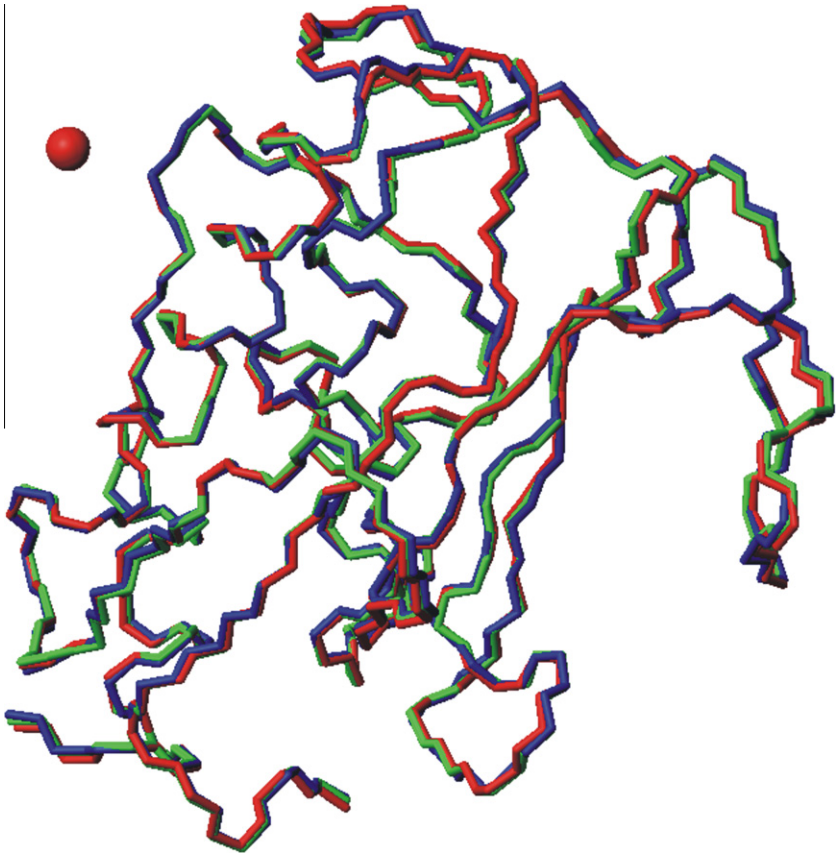

Fig. 5. Solution structure (red) superimposed to the crystal 1HFC structure (blue) and to the CYANA structure (green) calculated before the inclusion of the paramagnetic restraints. The red sphere shows the position of the paramagnetic metals.

[51,52], although a slight structural heterogeneity may likely be present. In fact, since all these solution models nicely satisfy the experimental restraints, any ensemble composed of these structures will also satisfy all restraints, as well as many other ensembles not containing any of them. However, it is clear that no physical meaning can be given to such ensembles. The concept that the number of structures needed to represent a molecule should be restricted to the minimum required by the experimental data is referred as an application of the Occam's razor [53].

The improvement in the accuracy of the solution structures can be monitored by comparing the dihedral angles of the structures before and after the inclusion of the paramagnetic restraints. Fig. 6 shows the differences in the ϕ dihedral angles among the three crystal structures (1HFC, 1CGE and 3SHI) as well as the differences with the corresponding solution structures. It can be seen that there are small but significant changes in these angles, which were necessary to adjust the rdc values to the experimental ones. These changes are in many cases consistently outside the range of the values of the crystal structures. This indicates that the paramagnetic data modify the ϕ dihedral angles in a way that is meaningful. The changes in the values of the ψ dihedral angles are minor and often within the variability of the different structures, as a result of the smaller effect of H–^{H}N vectors on these angles. The average difference of the ϕ dihedral angles between the starting structures and the corresponding solution ones is 9.1°, 10.8° and 10.8° for the 1HFC, 3SHI and 1CGE structures, respectively. As expected, the 1HFC structure, which was in best agreement with the rdc data, varied less to be in agreement with the experimental data.

The improvement in the accuracy of the solution structures was also verified by cross-validation with data not used in the calculations. In fact, if the latter are performed by removing the rdc measured for one metal of the residues for which rdc have been measured also for the other two metals (5 rdc values in total), the Q_{free} of these rdc is still small (0.23 versus 0.34 in the crystal structure). A similar decrease in the Q_{free} is observed when also the rdc measured for the residues of at least another metal, belonging to secondary structural elements (8 rdc values in total), are removed.

In conclusion, the paramagnetism-based restraints indicate that the solution structure of the catalytic domain of MMP-1 is in good agreement with the crystal structure and provide a tool for an improvement in solution of the orientation of the vectors for which rdc have been measured.

3.5. Proteins with solution structures different from the crystal structures

In the case of calmodulin, it was previously shown that the solution structure of the N-terminal domain differs from the crystal structure [4]. A crystal structure at high resolution (1 Å) is available (1EXR), as well as the rdc for H–^{H}N, H^{α}–C^{α}, C′–N, C^{α}–C′, H^{α}–C′ nuclear pairs, measured in liquid crystalline medium. The protocol described in the previous sections was applied to this system to check whether it correctly indicates that the NMR restraints are incompatible with the crystal structure unless large conformational changes are allowed. The best fit of the experimental rdc to the 1EXR structure is indeed quite unsatisfactory (Fig. 7A) and it does not improve sizably when the rdc data are introduced into the CYANA calculations (Fig. 7B): the Q factor, equal to 0.39 for the crystal structure, remains as high as 0.32 after the restrained minimization. Therefore, the approach itself indicates that the rdc are not compatible with any slightly modified crystal structure.

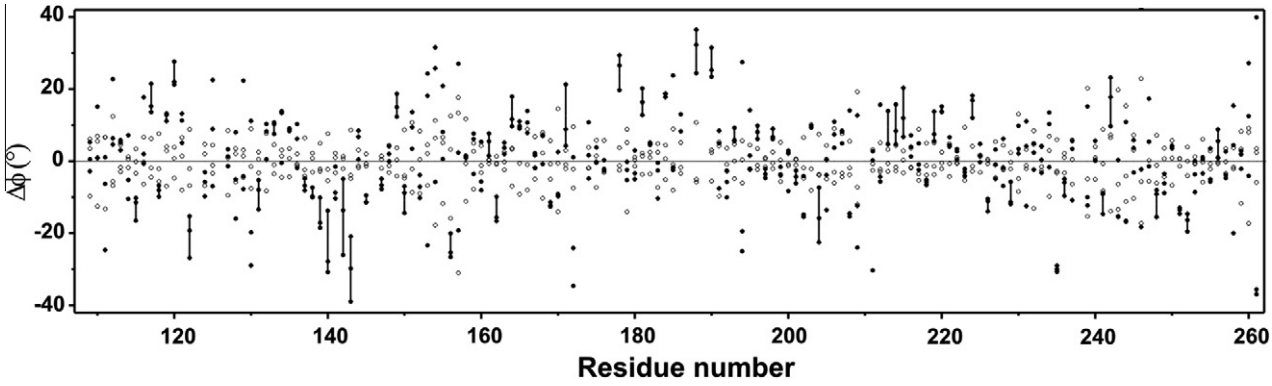

Fig. 6. Dihedral ϕ angles of the solution structures (solid symbols) and of the crystal structures (open symbols), after subtraction of the average of the angles calculated from the crystal structures. The bars indicate the residues whose dihedral angles in solution are consistently outside the range of the values observed at the solid state. The analyzed structures are the 1HFC, 3SHI and 1CGE structures.

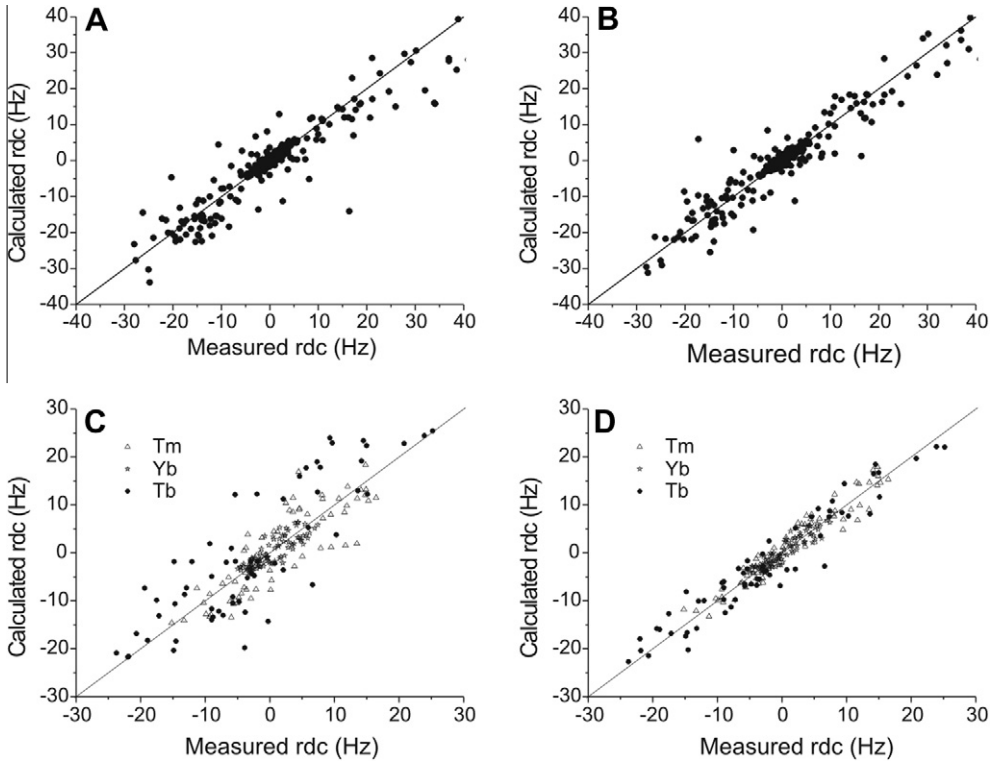

Fig. 7. (A) Best fit of the experimental rdc values to the crystal 1EXR structure of calmodulin and (B) to the structure calculated with the inclusion of the solution restraints. (C) Agreement between experimental rdc and rdc calculated from the pcs-derived tensors and the crystal 1YR5 structure of calmodulin bound to the binding peptide of DAPk or (D) the structure calculated with the inclusion of the paramagnetic restraints.

The agreement between the crystal structure and the paramagnetic restraints was also checked for the adduct of N60D calmodulin with the binding peptide of DAPk [5]. For this system, pcs and rdc were collected for the Yb^{3+}, Tb^{3+} and Tm^{3+} ions substituted to the second binding site of the N-terminal domain and used to show the occurrence of a conformational rearrangement involving the first helix of the N-terminal domain and the whole C-terminal domain with respect to the N-terminal domain [5]. Indeed, the agreement of the rdc data is modest (Fig. 7D, $Q = 0.28$; the Q factor of the pcs is 0.10), with differences up to 10 Hz between the calculated rdc and the experimental values, when the conformation of the protein is restrained to the coordinates of the crystal structure. Again, the protocol points to a sizable conformational rearrangement occurring on passing from crystal to solution. In these cases, previously described methods [2,4,5] should be applied for a structural refinement, based on the inclusion of dihedral angles restraints, which replace the distance restraints anchoring the nuclear coordinates to the model structure, and the inclusion of appropriate force fields for keeping the protein structure properly folded while allowing secondary structure or domain rearrangements.

4. Concluding remarks

Solid state structures are known to suffer from crystal packing forces so that they may not be accurate models for the structures in solution. Paramagnetism-assisted NMR can provide valuable restraints to assess the extent and the nature (local or global) of the deviations, and to produce better models for the solution

structures, without the need to assign all proton resonances and collect and analyze all the NMR spectra required for the collection of the classical NMR restraints. A protocol is presented for discriminating between the case of minor, local changes needed to reconcile the available model with the experimental data, and the case of major, global changes as those involving domain reorientations [54]. In the former case, the smallest structural changes that are needed to reproduce the experimental data can be determined and solution structures of improved accuracy are thus obtained. The tolerance and weight used for restraining the protein coordinates to the crystal model must be adjusted in order to allow a contribution to the target function of the NMR restraints low and comparable with the contribution of the upper distance limits anchoring the nuclear coordinates. If even with tolerances of few tenths of an Angstrom the NMR data cannot be reproduced within their error, the approaches developed for refining the proteins in the presence of major global changes, previously described [2,4,5], should be used.

These protocols are foreseen to be of large utility for the structural and dynamic characterization of protein complexes and of multidomain proteins, where the different domains have some degree of orientational freedom. In these cases, in fact, the paramagnetism-based restraints, collected thanks to the presence of paramagnetic metal ions rigidly positioned in one protein domain, can be used for determining the relative position of the protein domains with respect to one another in case of no motion, or for obtaining information on the conformational heterogeneity of the system in the presence of interdomain motion. Preliminary to this is, of course, the availability of the solution structures of each rigid protein domain. After checking the consistency of crystal and solution restraints, the simultaneous use of diffraction data and paramagnetic restraints for the structural calculation of a protein can be advantageous for obtaining structures of improved accuracy and precision, as also previously shown using classical NMR restraints [55].

Acknowledgements

This work has been supported by Fundação para a Ciência e Tecnologia (FCT), Portugal (grant SFRH/BD/45928/2008 to J.M.C.T.), MIUR-FIRB contracts RBLA032ZM7 and RBRN07BMCT, Ente Cassa di Risparmio di Firenze, and by the European Commission, contracts Bio-NMR n. 261863, East-NMR n. 228461, Strep-Sfmet n. 201640, and We-NMR 261572.

Appendix A. Supplementary data

Supplementary data associated with this article can be found, in the online version, at doi:10.1016/j.febslet.2011.09.020.

References

[1] Gochin, M. and Roder, H. (1995) Protein structure refinement based on paramagnetic NMR shifts. Applications to wild-type and mutants forms of Cytochrome c. Protein Sci. 4, 296–305.
[2] Chou, J.J., Li, S. and Bax, A. (2000) Study of conformational rearrangement and refinement of structural homology models by the use of heteronuclear dipolar couplings. J. Biomol. NMR 18, 217–227.
[3] Skrynnikov, N.R., Goto, N.K., Yang, D., Choy, W.-Y., Tolman, J.R., Mueller, G.A. and Kay, L.E. (2000) Orienting domains in proteins using dipolar couplings measured by liquid-state NMR: Differences in solution and crystal forms of maltodextrin binding protein loaded with β-cyclodextrin. J. Mol. Biol. 295, 1265–1273.
[4] Chou, J.J., Li, S., Klee, C.B. and Bax, A. (2001) Solution structure of Ca^{2+} calmodulin reveals flexible hand-like properties of its domains. Nature Struct. Biol. 8, 990–997.
[5] Bertini, I., Kursula, P., Luchinat, C., Parigi, G., Vahokoski, J., Willmans, M. and Yuan, J. (2009) Accurate solution structures of proteins from X-ray data and minimal set of NMR data: calmodulin peptide complexes as examples. J. Am. Chem. Soc. 131, 5134–5144.
[6] Bertini, I., Faraone-Mennella, J., Gray, B.H., Luchinat, C., Parigi, G. and Winkler, J.R. (2004) NMR-validated structural model for oxidized Rhodopseudomonas palustris cytochrome c556. J. Biol. Inorg. Chem. 9, 224–230.
[7] Fragai, M., Luchinat, C. and Parigi, G. (2006) "Four-dimensional" protein structures: examples from metalloproteins. Acc. Chem. Res. 39, 909–917.
[8] Bertini, I., Luchinat, C., Parigi, G. and Pierattelli, R. (2008) Perspectives in NMR of paramagnetic proteins. Dalton Trans. 2008, 3782–3790.
[9] Bertini, I., Gupta, Y.K., Luchinat, C., Parigi, G., Peana, M., Sgheri, L. and Yuan, J. (2007) Paramagnetism-based NMR restraints provide maximum allowed probabilities for the different conformations of partially independent protein domains. J. Am. Chem. Soc. 129, 12786–12794.
[10] Bertini, I., Giachetti, A., Luchinat, C., Parigi, G., Petoukhov, M.V., Pierattelli, R., Ravera, E. and Svergun, D.I. (2010) Conformational space of flexible biological macromolecules from average data. J. Am. Chem. Soc. 132, 13553–13558.
[11] Bertini, I., Fragai, M., Luchinat, C., Melikian, M., Mylonas, E., Sarti, N. and Svergun, D. (2009) Interdomain flexibility in full-lenght matrix metalloproteinase-1 (MMP-1). J. Biol. Chem. 284, 12821–12828.
[12] Su, X.C., Huber, T., Dixon, N.E. and Otting, G. (2006) Site-specific labelling of proteins with a rigid lanthanide-binding tag. ChemBioChem 7, 1599–1604.
[13] Keizers, P.H., Desreux, J.F., Overhand, M. and Ubbink, M. (2007) Increased paramagnetic effect of a lanthanide protein probe by two-point attachment. J. Am. Chem. Soc. 129, 9292–9293.
[14] Su, X.C., Man, B., Beeren, S., Liang, H., Simonsen, S., Schmitz, C., Huber, T., Messerle, B.A. and Otting, G. (2008) A dipicolinic acid tag for rigid lanthanide tagging of proteins and paramagnetic NMR spectroscopy. J. Am. Chem. Soc. 130, 10486–10487.
[15] Vlasie, M.D., Fernández-Busnadiego, R., Prudêncio, M. and Ubbink, M. (2008) Conformation of pseudoazurin in the 152 kDa electron transfer complex with nitrite reductase determined by paramagnetic NMR. J. Mol. Biol. 375, 1405–1415.
[16] Zhuang, T., Lee, H.S., Imperiali, B. and Prestegard, J.H. (2008) Structure determination of a Galectin-3-carbohydrate complex using paramagnetism-based NMR constraints. Protein Sci. 17, 1220–1231.
[17] Xu, X., Keizers, P.H.J., Reinle, W., Hannemann, F., Bernhardt, R. and Ubbink, M. (2009) Intermolecular dynamics studied by paramagnetic tagging. J. Biomol. NMR 43, 247–254.
[18] Saio, T., Ogura, K., Yokochi, M., Kobashigawa, Y. and Inagaki, F. (2009) Two-point anchoring of a lanthanide-binding peptide to a target protein enhances the paramagnetic anisotropic effect. J. Biomol. NMR 44, 157–166.
[19] Häussinger, D., Huang, J. and Grzesiek, S. (2009) DOTA-M8: an extremely rigid, high-affinity lanthanide chelating tag for PCS NMR spectroscopy. J. Am. Chem. Soc. 131, 14761–14767.
[20] Hass, M.A.S., Keizers, P.H.J., Blok, A., Hiruma, Y. and Ubbink, M. (2010) Validation of a lanthanide tag for the analysis of protein dynamics by paramagnetic NMR spectroscopy. J. Am. Chem. Soc. 132, 9952–9953.
[21] Man, B., Su, X.C., Liang, H., Simonsen, S., Huber, T., Messerle, B.A. and Otting, G. (2010) 3-Mercapto-2,6-pyridinedicarboxylic acid: a small lanthanide-binding tag for protein studies by NMR spectroscopy. Chem. Eur. J. 16, 3827–3832.
[22] Keizers, P.H.J., Saragliadis, A., Hiruma, Y., Overhand, M. and Ubbink, M. (2008) Design, synthesis, and evaluation of a lanthanide chelating protein probe: CLaNP-5 yields predictable paramagnetic effects independent of environment. J. Am. Chem. Soc. 130, 14802–14812.
[23] Keizers, P.H.J., Mersinli, B., Reinle, W., Donauer, J., Hiruma, Y., Hannemann, F., Overhand, M., Bernhardt, R. and Ubbink, M. (2010) A solution model of the complex formed by adrenodoxin and adrenodoxin reductase determined by paramagnetic NMR spectroscopy. Biochemistry 49, 6846–6855.
[24] Polášek, M., Šedinová, M., Kotek, J., Vander Elst, L., Muller, R.N., Hermann, P. and Lukeš, I. (2009) Pyridine-N-oxide analogues of DOTA and their Gadolinium(III) complexes endowed with a fast water exchange on the square-antiprismatic isomer. Inorg. Chem. 48, 455–465.
[25] Bertini, I., Fragai, M., Giachetti, A., Luchinat, C., Maletta, M., Parigi, G. and Yeo, K.J. (2005) Combining in silico tools and NMR data to validate protein-ligand structural models: application to matrix metalloproteinases. J. Med. Chem. 48, 7544–7559.
[26] Leslie, A.G.W. (1991) In crystallographic computing V in: Molecular Data Processing (Moras, D., Podjarny, A.D. and Thierry, J.-C., Eds.), pp. 50–61, Oxford University Press, Oxford.
[27] Evans PR. Data reduction. In: Proceedings of CCP4 Study Weekend. Data Collection & Processing, 1993. p. 114–122
[28] Rossmann, M.G. and Blow, D.M. (1962) The detection of sub-units within the crystallographic asymmetric unit. Acta Cryst. D15, 24–31.
[29] Crowther, R.A. (1972) The Molecular Replacement Method. In: Rossmann, M.G., editor. Gordon & Breach, New York.
[30] Vagin, A.A. and Teplyakov, A. (1997) MOLREP: an automated program for molecular replacement. J. Appl. Crystallogr. 30, 1022–1025.
[31] Vagin, A.A. and Teplyakov, A. (2000) An approach to multi-copy search in molecular replacement. Acta Crystallogr. D: Biol. Crystallogr. 56, 1622–1624.
[32] Murshudov, G.N., Vagin, A.A. and Dodson, E.J. (1997) Refinement of macromolecular structures by the maximum-likelihood method. Acta Crystallogr. D: Biol. Crystallogr. 53, 240–255.
[33] McRee, D.E. (1992) XtalView: a visual protein crystallographic software system for XII/XView. J. Mol. Graphics 10, 44–47.
[34] Lamzin, V.S. and Wilson, K.S. (1993) Automated refinement of protein models. Acta Crystallogr. D: Biol. Crystallogr. 49, 129–147.
[35] Laskowski, R.A., MacArthur, M.W., Moss, D.S. and Thornton, J.M. (1993) PROCHECK: a program to check the stereochemical quality of protein structures. J. Appl. Crystallogr. 26, 283–291.

[36] Keller R (2003) The CARA/Lua Programmers Manual. DATONAL AG.
[37] Moy, F.J., Pisano, M.R., Chanda, P.K., Urbano, C., Killar, L.M., Sung, M.L. and Powers, R. (1997) Assignments, secondary structure and dynamics of the inhibitor-free catalytic fragment of human fibroblast collagenase. J. Biomol. NMR 10, 9–19.
[38] Ottiger, M., Delaglio, F. and Bax, A. (1998) Measurement of J and dipolar couplings from simplified two-dimensional NMR spectra. J. Magn. Reson. 131, 373–378.
[39] Bertini, I., Luchinat, C. and Parigi, G. (2002) Magnetic susceptibility in paramagnetic NMR. Progr. NMR Spectrosc. 40, 249–273.
[40] Banci, L., Bertini, I., Huber, J.G., Luchinat, C. and Rosato, A. (1998) Partial orientation of oxidized and reduced cytochrome b_5 at high magnetic fields: Magnetic susceptibility anisotropy contributions and consequences for protein solution structure determination. J. Am. Chem. Soc. 120, 12903–12909.
[41] Tolman, J.R., Flanagan, J.M., Kennedy, M.A. and Prestegard, J.H. (1995) Nuclear magnetic dipole interactions in field-oriented proteins: information for structure determination in solution. Proc. Natl. Acad. Sci. USA 92, 9279–9283.
[42] Tolman, J.R., Flanagan, J.M., Kennedy, M.A. and Prestegard, J.H. (1997) NMR evidence for slow collective motions in cyanometmyoglobin. Nature Struct. Biol. 4, 292–297.
[43] Bax, A. and Tjandra, N. (1997) Are proteins even floppier than we thought? Nature Struct. Biol. 4, 254–256.
[44] Bothner-By, A.A., Domaille, J.P. and Gayathri, C. (1981) Ultra high-field NMR spectroscopy: observation of proton-proton dipolar coupling in paramagnetic bis[tolyltris(pyrazolyl)borato]cobalt(II). J. Am. Chem. Soc. 103, 5602–5603.
[45] Bertini, I., Luchinat, C., Parigi, G. and Pierattelli, R. (2005) NMR of paramagnetic metalloproteins. ChemBioChem 6, 1536–1549.
[46] Guntert, P. (2004) Automated NMR structure calculation with CYANA. Methods Mol. Biol. 278, 353–378.
[47] Balayssac, S., Bertini, I., Luchinat, C., Parigi, G. and Piccioli, M. (2006) ^{13}C direct detected NMR increases the detectability of residual dipolar couplings. J. Am. Chem. Soc. 128, 15042–15043.
[48] Bertini, I., Luchinat, C. and Parigi, G. (2011) Moving the frontiers in solution solid state bioNMR. A celebration of Harry Gray's 75th birthday. Coord. Chem. Rev. 255, 649–663.
[49] Banci, L., Bertini, I., Cavallaro, G., Giachetti, A., Luchinat, C. and Parigi, G. (2004) Paramagnetism-based restraints for Xplor-NIH. J. Biomol. NMR 28, 249–261.
[50] Barbieri, R., Luchinat, C. and Parigi, G. (2004) Backbone-only protein solution structures with a combination of classical and paramagnetism-based constraints: a method that can be scaled to large molecules. ChemPhysChem 21, 797–806.
[51] Clore, G.M. and Schwieters, C.D. (2006) Concordance of residual dipolar couplings, backbone order parameters and crystallographic B-factors for a small α/β protein: a unified picture of high probability, fast motions in proteins. J. Mol. Biol. 355, 879–886.
[52] Lange, O.F., Lakomek, N.-A., Farès, C., Schröder, G.F., Walter, K.F.A., Becker, S., Meiler, J., Grubmüller, H., Griesinger, C. and de Groot, B.L. (2008) Recognition dynamics up to microseconds revealed from an RDC-derived ubiquitin ensemble in solution. Science 320, 1471–1475.
[53] Clore, G.M. and Schwieters, C.D. (2004) How much backbone motion in ubiquitin is required to account for dipolar coupling data measured in multiple alignment media as assessed by independent cross-validation? J. Am. Chem. Soc. 126, 2923–2938.
[54] Clore, G.M. and Kuszewski, J. (2003) Improving the accuracy of NMR structures of RNA by means of conformational database potentials of mean force as assessed by complete dipolar coupling cross-validation. J. Am. Chem. Soc. 125, 1518–1525.
[55] Shaanan, B., Gronenborn, A.M., Cohen, G.H., Gilliland, G.L., Veerapandian, B., Davies, D.R. and Clore, G.M. (1992) Combining experimental information from crystal and solution studies – joint X-ray and NMR refinement. Science 257, 961–964.